available at www.sciencedirect.com
journal homepage: www.europeanurology.com

European Association of Urology

Platinum Priority – Brief Correspondence

Editorial by Claire E. Fletcher on pp. 167–169 of this issue

RNA Splicing of the *BHC80* Gene Contributes to Neuroendocrine Prostate Cancer Progression

Yinan Li[a], *Ning Xie*[a], *Ruiqi Chen*[a], *Ahn R. Lee*[a], *Jessica Lovnicki*[a], *Emma A. Morrison*[b], *Ladan Fazli*[a], *Qingfu Zhang*[c,d], *Catherine A. Musselman*[b], *Yuzhuo Wang*[a], *Jiaoti Huang*[c], *Martin E. Gleave*[a], *Colin Collins*[a], *Xuesen Dong*[a,*]

[a] *Vancouver Prostate Centre, Department of Urologic Sciences, University of British Columbia, Vancouver, BC, Canada;* [b] *Department of Biochemistry, Carver College of Medicine, University of Iowa, Iowa City, IA, USA;* [c] *Department of Pathology, Duke University School of Medicine, Durham, NC, USA;* [d] *China Medical University, Shenyang, China*

Article info

Article history:
Accepted March 8, 2019

Associate Editor:
Matthew Cooperberg

Statistical Editor:
Andrew Vickers

Keywords:
Treatment-induced neuroendocrine prostate cancer
Alternative RNA splicing
BHC80
SRRM4

Abstract

Background: Prostate adenocarcinoma (AdPC) progression to treatment-induced neuroendocrine prostate cancer (t-NEPC) is associated with poor patient survival. While AdPC and t-NEPC share similar genomes, they possess distinct transcriptomes, suggesting that RNA splicing and epigenetic mechanisms may regulate t-NEPC development.
Objective: To characterize the role of alternative RNA splicing of the histone demethylase BHC80 during t-NEPC progression.
Design, setting, and participants: The expression of BHC80 splice variants (BHC80-1 and BHC80-2) were compared between AdPC and t-NEPC patient tumors. Regulatory mechanisms of RNA splicing of the *BHC80* gene were studied, and the signal pathways mediated by BHC80 splice variants were investigated in t-NEPC cell and xenograft models.
Results: Global transcriptome analyses identified that the BHC80-2 variant is highly expressed in t-NEPC. Compared with the known histone demethylation activities of the *BHC80* gene, we discovered a novel nonepigenetic action of BHC80-2, whereby BHC80-2 is localized in the cytoplasm to trigger the MyD88-p38-TTP pathway, which results in increased RNA stability of multiple tumor-promoting cytokines. While BHC80-2 does not induce neuroendocrine differentiation of cancer cells, it stimulates cell proliferation and tumor progression independent of androgen receptor signaling. Blockade of BHC80-2-regulated MyD88 signaling suppresses growth of several t-NEPC cell spheroid and xenograft models.
Conclusions: Gain of function of BHC80-2 through alternative RNA splicing activates immune responses of cancer cells to promote t-NEPC development.
Patient summary: The main obstacle to develop effective therapies for patients with t-NEPC is the lack of understanding on how t-NEPC is developed. Our study not only identifies a previously unknown BHC80-2-MyD88 signaling pathway that plays an important role during t-NEPC development, but also provides a proof of principle that targeting this signal pathway may offer an avenue to treat t-NEPC.

* Corresponding author. Vancouver Prostate Centre, Department of Urologic Sciences, University of British Columbia, 2660 Oak Street, Vancouver, BC V6H 3Z6, Canada. Tel. +1 604 875 4111; Fax: +1 604 875 5654.
E-mail address: xdong@prostatecentre.com (X. Dong).

https://doi.org/10.1016/j.eururo.2019.03.011

1. Introduction

Treatment-induced neuroendocrine prostate cancer (t-NEPC) is becoming more prevalent under the selective pressures of more potent androgen receptor (AR) pathway inhibition [1]. Once t-NEPC is diagnosed, patient survival is <1 yr [2]. While 10–100% of prostate cancer (PCa) patients were reported to have tumor cells with neuroendocrine (NE) differentiation [3], only ~25% of patients with advanced prostate tumors eventually develop aggressive t-NEPC [4]. These findings imply that only NE tumor cells that attain a proliferative state will develop into t-NEPC. However, the molecular underpinning of t-NEPC development remains unclear.

Treatment-induced NEPC is most often derived from prostate adenocarcinoma (AdPC) through the complex interplay of NE differentiation, proliferation, and oncogenic processes. Whole-exome sequencing has revealed that t-NEPC and AdPC share similar genomic landscapes, even though they differ significantly in transcriptome and cell morphology [1,5]. Case studies show that cell populations of AdPC, AdPC with NE differentiation, and t-NEPC coexist in the same tumors [5]. Intermediate morphological and phenotypical transitions in cancer cells between the boundaries of AdPC and NEPC cell populations indicate a dynamic NE differentiation process [5]. AdPC transformation into t-NEPC is replicable in patient-derived xenografts (PDXs) only after castration surgery in host mice [6]. Loss of function of TP53, Rb1, and/or PTEN can confer lineage plasticity to AdPC cells under anti-AR treatment [7–10]. These cancer cells may utilize Sox2, EZH2, and Sox11 to epigenetically reprogram the AdPC transcriptome to adapt into an NE lineage. AdPC cells can be transformed into t-NEPC xenografts by a neural RNA splicing factor, SRRM4, introduced exogenously [11–13]. These findings support that t-NEPC likely originates from AdPC.

AdPC progression to t-NEPC requires both NE differentiation and cell proliferation. NE differentiation can be induced by the loss of function of AR, REST, or FOXA1, or by treatments of cAMP, IL-6, or hypoxia in vitro [11,14–17]. However, not all these factors enable t-NEPC tumorigenesis. While AR blockade is necessary for t-NEPC establishment, it is not always sufficient because only ~25% of hormone therapy-treated tumors gain t-NEPC phenotypes [4]. The majority of AR-positive AdPC xenografts (eg, LNCaP and LAPC4) do not progress to t-NEPC by castration. When TP53/PTEN knockout mice were treated with castration surgery, NE-like cells from focal NE differentiation regions were nonproliferative, in contrast to NE-like cells within overt NE differentiation regions that were highly proliferative [8], suggesting that a "proliferative switch" is a key molecular event that enables t-NEPC development. Genes such as *AURKA*, *PEG10*, *MEAF6*, and *CyclinD1* have been implicated in t-NEPC development [18,19]. However, instead of inducing NE differentiation of AdPC cells, they regulate cell proliferation and tumor growth. These findings support that AdPC cells with NE differentiation have to be switched into a highly proliferative state in order for t-NEPC establishment.

While AdPC and t-NEPC share similar genomic features, their transcriptomes differ dramatically, suggesting that RNA splicing and epigenetic mechanisms play key roles in t-NEPC development. By analyzing RNA-seq data from two independent NEPC cohorts [6,20], we reported a t-NEPC-specific RNA splicing signature [11]. *BHC80* is the only gene that regulates histone demethylation and thereby gene transcription [21]. It is expressed as two isoforms (BHC80-1 and BHC80-2) whereby an alternative exon14a replaces exon14 in BHC80-2 (GRCh38/hg38) [22]. This splicing event disrupts one of the predicted nuclear localization signals (NLSs), potentially leading to cytoplasmic localization. This study aims to characterize BHC80-2 splicing in t-NEPC.

2. Patients and methods

The patients included and methods used in this study are described in the Supplementary material.

3. Results

3.1. RNA splicing of BHC80-2 is upregulated in t-NEPC

RNA-seq data from both the VPC and the Beltran cohorts [1,11] indicated that BHC80-2 is expressed at extremely low levels in AdPC but dramatically induced in t-NEPC, while BHC80-1 levels are similar between AdPC and t-NEPC (Supplementary Fig. 1A and B). To validate these findings, we constructed a tissue microarray (TMA) containing 64 castration-resistant prostate cancer (CRPC) tumor cores and applied RNA in situ hybridization (RISH) assays. We confirmed that BHC80-2 was strongly expressed in two subtypes of t-NEPC, namely, small cell neuroendocrine carcinoma (SCNC) and AdPC with abundant NE cells (AdNE) [23], but lowly expressed in AdPC (Fig. 1A–C). In contrast, BHC80-1 expression showed no difference among all tumor groups. The specificity of the BHC80-1 and BHC80-2 probes was validated by multiple control slides (Supplementary Fig. 2). The RISH signal of BHC80-2, but not of BHC80-1, was positively correlated with the number of NE markers ($p < 0.001$) and the immunohistochemistry (IHC) scores of CHGA, SYP, and CD56 ($p < 0.001$; Fig. 1D and E, and Supplementary Figs. 3 and 4). These findings are consistent with the RNA-seq results from the Beltran 2016 cohort (Supplementary Fig. 5). AdNE tumors had a much lower Ki67 index than SCNC, suggesting that they had undergone NE differentiation but not yet switched to high proliferative states as in SCNC (Fig. 1B and C). BHC80-2 was negatively correlated with AdPC markers such as AR and prostate-specific antigen (PSA; Fig. 1E). Together, both RNA-seq and RISH results from three independent patient cohorts support that BHC80-2 is upregulated in t-NEPC, while BHC80-1 expression remains similar between AdPC and t-NEPC.

3.2. SRRM4 regulates RNA splicing of BHC80-2

Since the RNA splicing factor SRRM4 has been demonstrated to drive t-NEPC progression, we hypothesized that SRRM4 regulates BHC80-2 RNA splicing. RNA-seq data from the Beltran 2016 cohort showed that BHC80-2 expression

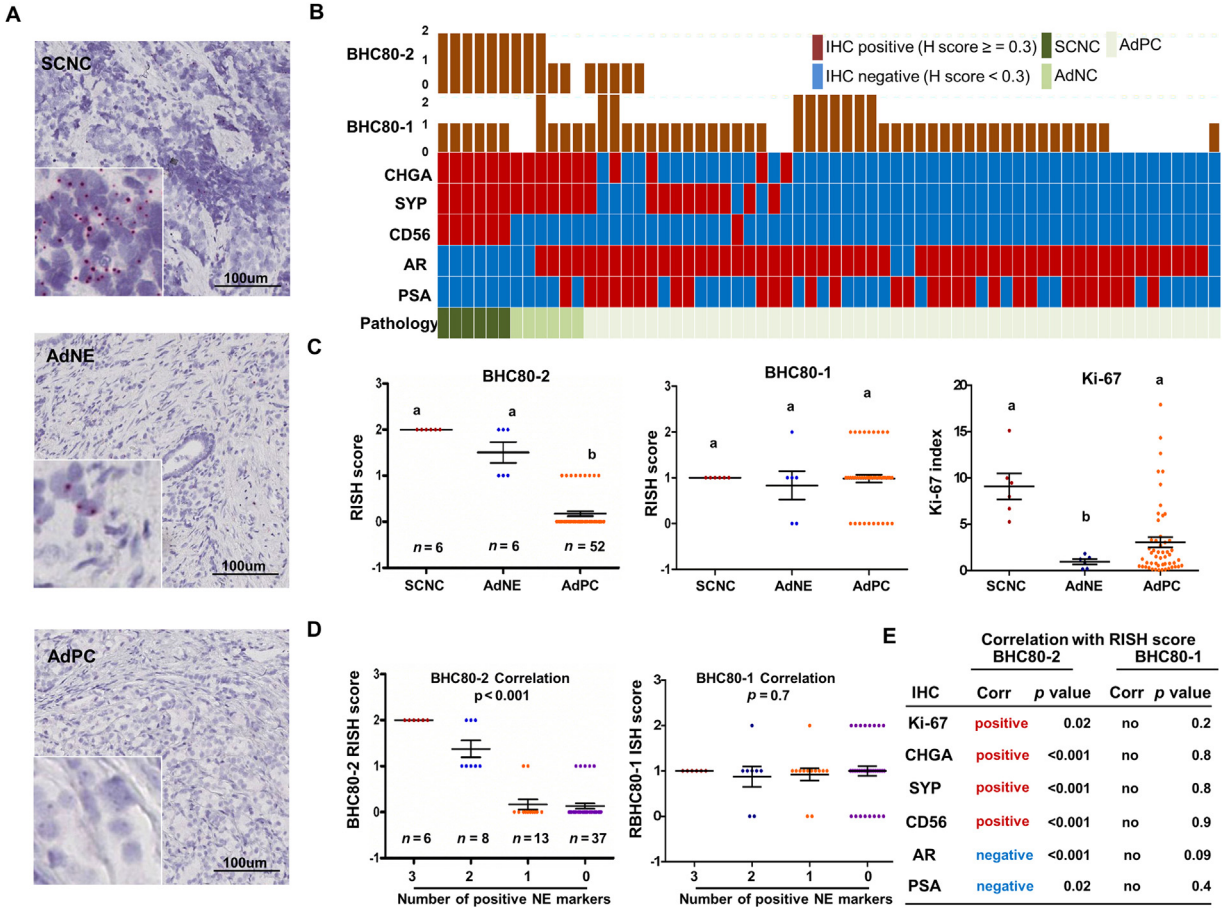

Fig. 1 – RNA splicing of BHC80-2 is upregulated in t-NEPC. BHC80-1 and BHC80-2 RISH assays, and CHGA, SYP, CD56, AR, PSA, and Ki-67 IHC assays were performed on the CRPC TMA, as previously described [23]. (A) Representative images of BHC80-2 RISH staining are shown. (B) RISH scores of BHC80-1 and BHC80-2; IHC scores of CHGA, SYP, CD56, AR, and PSA; and pathology classification of the tumor cores are presented. Each column shows data from the same tissue core. (C) CRPC tissue cores are grouped into SCNC, AdNE, and AdPC according their histology [23]. Distributions of BHC80-1 and BHC80-2 RISH scores as well as Ki-67 index of each tumor group are plotted. (D) Associations of BHC80-1 and BHC80-2 RISH scores with the numbers of CHGA, SYP, and CD56 positivity per core on the whole CRPC TMA were calculated by Pearson's chi-square test. (E) BHC80-2 expression in correlation with CHGA, SYP, CD56, AR, and PSA IHC scores and Ki-67 index was calculated by Pearson's chi-square test. Data are presented as the mean ± SEM. Values without a common letter are significantly different ($p < 0.05$). AdNE = AdPC with abundant neuroendocrine cells; AdPC = prostate adenocarcinoma; AR = androgen receptor; Corr = correlated; CRPC = castration-resistant prostate cancer; IHC = immunohistochemistry; NE = neuroendocrine; PSA = prostate-specific antigen; RISH = RNA in situ hybridization; SCNC = small cell neuroendocrine carcinoma; SEM = standard error of the mean; TMA = tissue microarray; t-NEPC = treatment-induced neuroendocrine prostate cancer.

was highly correlated with SRRM4 ($p < 0.001$; Fig. 2A). SRRM4 expression on the CRPC TMA had previously been reported [23]. Here, we further showed that BHC80-2 and SRRM4 RISH signals were high in both SCNC and AdNE, but low in AdPC ($p < 0.001$; Fig. 2B and Supplementary Fig. 6). These findings were consistent with BHC80-2 and SRRM4 protein expressions that were specific to NEPC PDXs (Fig. 2C). We recently established two SRRM4-driven t-NEPC cell models, LnNE and DuNE, which show not only global gene signature and morphological alterations, but also tumor progression mimicking patient t-NEPC [12,13]. BHC80-2 was negative in parental LNCaP and Du145 xenografts, but dramatically upregulated in LnNE and DuNE tumors (Fig. 2D and Supplementary Fig. 7). While BHC80-1 was universally expressed in all PCa cell lines, BHC80-2 was expressed only in SRRM4-positive NCI-H660 and VCaP lines (Fig. 2E). VCaP cells are both AR and SRRM4 positive due to gene amplification [11]. Together, these results establish a correlation of SRRM4 expression with BHC80-2 splicing.

To confirm that SRRM4 regulates BHC80-2 splicing, we showed that depletion of SRRM4 by siRNA in LnNE and DuNE cells resulted in the downregulation of BHC80-2, but not BHC80-1 mRNA levels (Supplementary Fig. 8A). We also constructed a BHC80 minigene reporter in which exons 14, 14a, and their flanking ~300 bp nucleotides were inserted between exons 13 and 15 (Fig. 2F) and transfected into LNCaP and 293T cells. SRRM4 upregulated BHC80-2 but downregulated BHC80-1 mRNA derived from the minigene reporter (Fig. 2G and Supplementary Fig. 8B). Interestingly, U2AF65 stimulated and PTB inhibited BHC80-2, but not BHC80-1 splicing, indicating that other splicing factors also regulate BHC80-2 splicing. However, SRRM4 is a neural-specific splicing factor that also regulates PTB RNA splicing

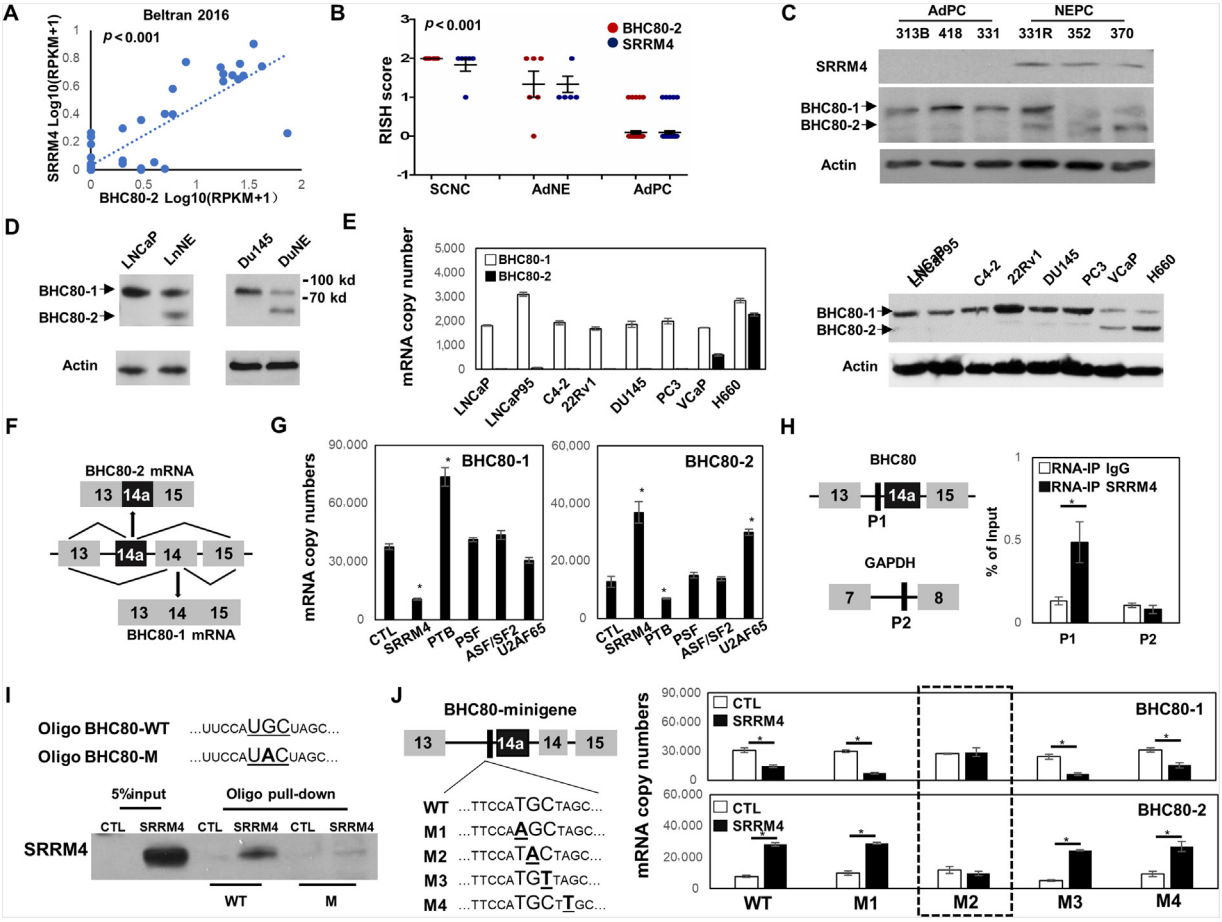

Fig. 2 – SRRM4 regulates RNA splicing of BHC80-2. (A) RNA-seq reads of the Beltran 2016 cohort are mapped with Star using Ensembl gene annotations GRCh38.87. Levels of mRNA expression were calculated as Log_{10}(RPKM + 1). The correlation of BHC80-2 with SRRM4 mRNA levels was calculated by Pearson's chi-square test. (B) The correlation of BHC80-2 and SRRM4 RISH scores on the CRPC TMA was calculated by Pearson's chi-square test. Data are presented as the mean ± SEM. (C) Protein lyses were extracted from three AdPC and three NEPC PDXs, and immunoblotted with SRRM4 and BHC80 antibodies. (D) LnNE and DuNE tumor samples were used to measure BHC80-1 and BHC80-2 protein expression by immunoblotting. (E) Multiple PCa cell models were used to measure BHC80-1, BHC80-2, and SRRM4 expression by real-time PCR and immunoblotting assays. (F and G) A schematic diagram shows the BHC80 minigene reporter and the derived splice variants. The BHC80 minigene reporter was cotransfected with plasmids encoding, indicating splicing factors in LNCaP cells. Total RNA was extracted to measure BHC80-1 and BHC80-2 mRNA levels by real-time qPCR. (H) A schematic diagram shows the P1 and P2 regions used in in vivo RNA binding assays. RNA-protein complexes in NCI-H660 cells were cross linked by formaldehyde, and immunoprecipitated with control or SRRM4 antibody. Eluted RNA fragments were used as templates for real-time qPCR to amplify the P1 and P2 regions. Signals were calculated as percentage of input. (I) Biotin-labeled RNA oligos containing wild-type and mutant UGC motifs were incubated with streptavidin conjugated beads. They were used to pull down protein extracts from NCI-H660 cells. Proteins associated with streptavidin beads were eluted and immunoblotted with an SRRM4 antibody. (J) LNCaP cells were transfected with control, BHC80 minigene or BHC80 minigene with M1–M4 mutations in the presence of −/+ SRRM4 plasmid. Total RNA was collected and used to measure BHC80-1 and BHC80-2 mRNA levels by real-time qPCR. All immunoblotting, real-time PCR, and RNA binding assays were repeated in three independent experiments that were performed in triplicate. Data are presented as the mean ± SD. * Delegates $p < 0.01$ when comparing with controls. One-way ANOVA followed by Tukey test was used in pairwise comparison among different groups. AdNE = AdPC with abundant neuroendocrine cells; AdPC = prostate adenocarcinoma; ANOVA = analysis of variance; CRPC = castration-resistant prostate cancer; NEPC = neuroendocrine prostate cancer; PCa = prostate cancer; PCR = polymerase chain reaction; PDX = patient-derived xenograft; qPCR = quantitative PCR; RISH = RNA in situ hybridization; SCNC = small cell neuroendocrine carcinoma; SD = standard deviation; SEM = standard error of the mean; TMA = tissue microarray.

and functions [24], leading us to focus on SRRM4-mediated BHC80-2 splicing. In vivo RNA binding assays showed that SRRM4 was recruited to the region next to the 3′ splice site of BHC80 intron 14 (P1 region), but not the control P2 region (Fig. 2H and Supplementary Fig. 8C). The UGC motif was predicted to be a consensus SRRM4 recognition site [25], and RNA pull-down assays confirmed that SRRM4 protein from NCI-H660 and 293T cells interacted with the wild type, but not the mutant UGC motif within the intron 14 (Fig. 2I and Supplementary Fig. 8D). Site-directed mutagenesis (UGC to UAC) within the BHC80 minigene showed failure of SRRM4-mediated exon14a inclusion (Fig. 2J and Supplementary Fig. 8E). These results confirmed that SRRM4 regulates BHC80-2 splicing.

3.3. *BHC80-2 promotes PCa cell growth and tumor progression androgen independently*

As BHC80-2 is barely expressed in AdPC but strongly induced in t-NEPC, we introduced Flag-tagged BHC80-2 into LNCaP, PC3, and TRAMP-C1 cells by lentivirus to study BHC80-2 functions (Supplementary Fig. 9). BHC80 isoforms

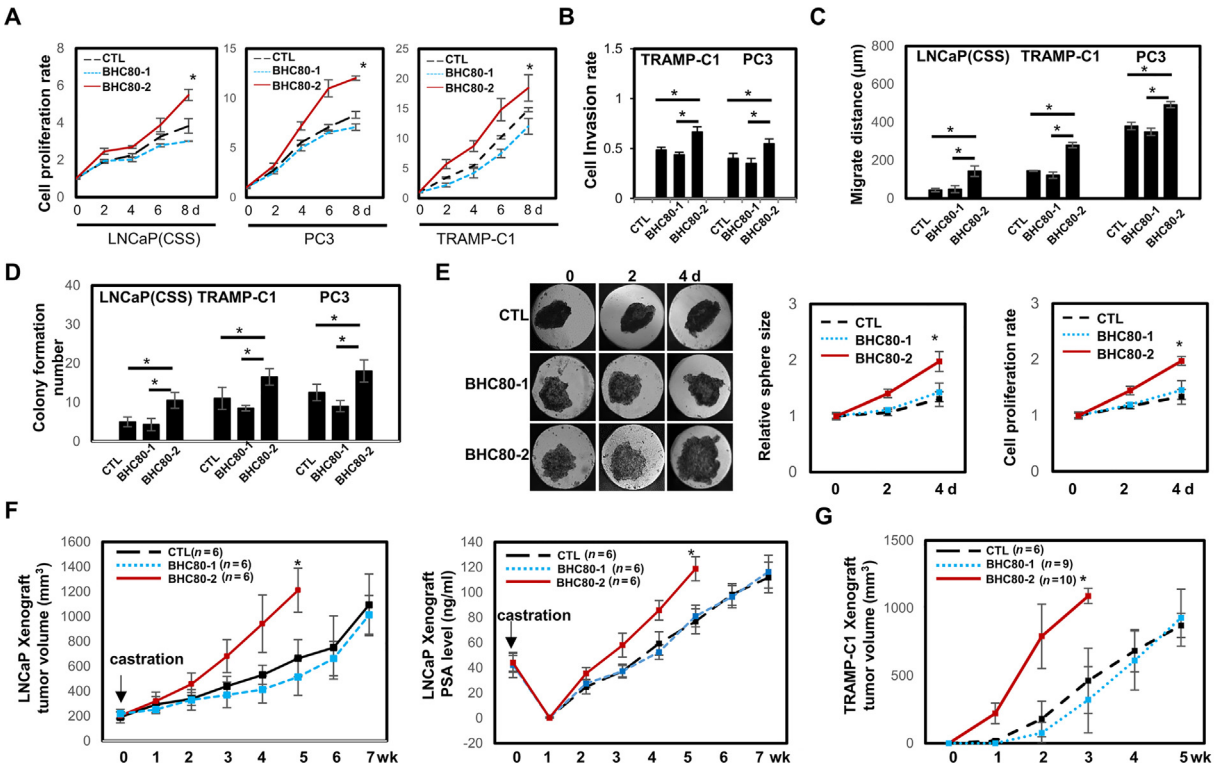

Fig. 3 – BHC80-2 promotes PCa cell growth and tumor progression androgen independently. (A) LNCaP, PC3, and TRAMP-C1 cell lines were stably transduced by control, BHC80-1, and BHC80-2 lentivirus. LNCaP cells were cultured under androgen-depleted conditions. Cell proliferation rates were measured by MTS assays and presented as relative fold change to day 0. (B) Cell invasion assays, described in the Supplementary material, were used to measure PC3 and TRAMP invasion capacity using the Matrigel invasion chambers. Cells invaded through the Matrigel layer were stained by crystal violet and counted using the ImageJ software. Invasion rates were calculated as the percentage of cells invaded through the Matrigel. (C) Wound healing assays were performed as described in the Supplementary material to measure PC3 and TRAMP-C1 cell migration rates within 16 h and LNCaP cell migration rate within 24 h. Cell images were captured by a Zeiss fluorescent microscope, and migration distances between 0 and 16 h time points were measured using the ImageJ software. (D) Colony formation assays were performed using 2×10^4 cells seeded in 0.7% soft agar in six-well plates. Cells were allowed to grow for 14 d to form colonies. Colonies were stained with crystal violet and imaged by stitching 5× field images together to capture the entire well (Zeiss light microscope; Carl Zeiss). Colony numbers were counted according to their diameters (>100 μm). Three independent biological replicates were performed for all the assays (Fig. 3A–D). All results are presented as the mean ± SD with * delegating $p < 0.01$. (E) LNCaP (CTL), LNCaP(BHC80-1), and LNCaP(BHC80-2) cells were cultured to form 3D multicellular spheroids as described in the Supplementary material. Time-lapse images are presented. Relative changes in spheroids sizes and proliferation rates were measured for 0–4 d. (F) LNCaP xenografts were established as described in the Supplementary material. Tumor volume and serum PSA concentrations are plotted. (G) TRAMP-C1 xenografts were established and tumor volumes were measured. One-way ANOVA followed by Tukey test was used in pairwise comparison among different experiment groups. ANOVA = analysis of variance; PCa = prostate cancer; PSA = prostate-specific antigen.

neither altered AR signaling, nor induced NE markers and neuronal morphologies (Supplementary Fig. 10). However, BHC80-2 but not BHC80-1 stimulated cell proliferation, migration, invasion, and colony formation independent of androgens in LNCaP, PC3, and TRAMP cells (Fig. 3A–D). LNCaP(BHC80-2) spheroids showed faster growth under three-dimensional (3D) conditions demonstrated by spheroid sizes and proliferation rates (Fig. 3E). LNCaP(BHC80-2) xenografts progressed more rapidly to castrate-resistant stage, demonstrated by tumor volumes and serum PSA levels (Fig. 3F). As >28-wk-old TRAMP mice develop poorly differentiated NEPC tumors attributed to the SV40 antigen that compromises Rb1 and TP53 functions [26], TRAMP-C1 cells were used as an NEPC prone model. BHC80-2 stimulated TRAMP-C1 xenograft growth (Fig. 3G, and Supplementary Fig. 9C and D). Furthermore, BHC80-2 knockout by CRISPR in the LnNE and DuNE models resulted in suppression of cell proliferation, migration, and invasion rates (Supplementary Fig. 11). Collectively, these results indicate that BHC80-2 stimulates PCa cell growth and xenograft progression androgen independently.

3.4. *BHC80-2 activates MyD88 signaling*

To decipher the BHC80-2 signaling pathway, we first profiled the BHC80-2 transcriptome using gene microarray analyses. While 3119 genes were differentially expressed in LNCaP(BHC80-2) cells compared with LNCaP(CTL) cells, 349 genes were differentially expressed between LNCaP (BHC80-1) and LNCaP(BHC80-2) cells ($p < 0.05$, fold change >2; Supplementary Fig. 12A). A total of 177 genes were specifically regulated by BHC80-2. Gene ontology (GO) analysis (http://david.abcc.ncifcrf.gov/) revealed that the key cellular processes were mainly related to immune response, antiapoptosis, and cell migration (Supplementary Fig. 12A–E). Seven GO annotation function groups were enriched, and the expression of representative genes within these groups was plotted. The BHC80-2

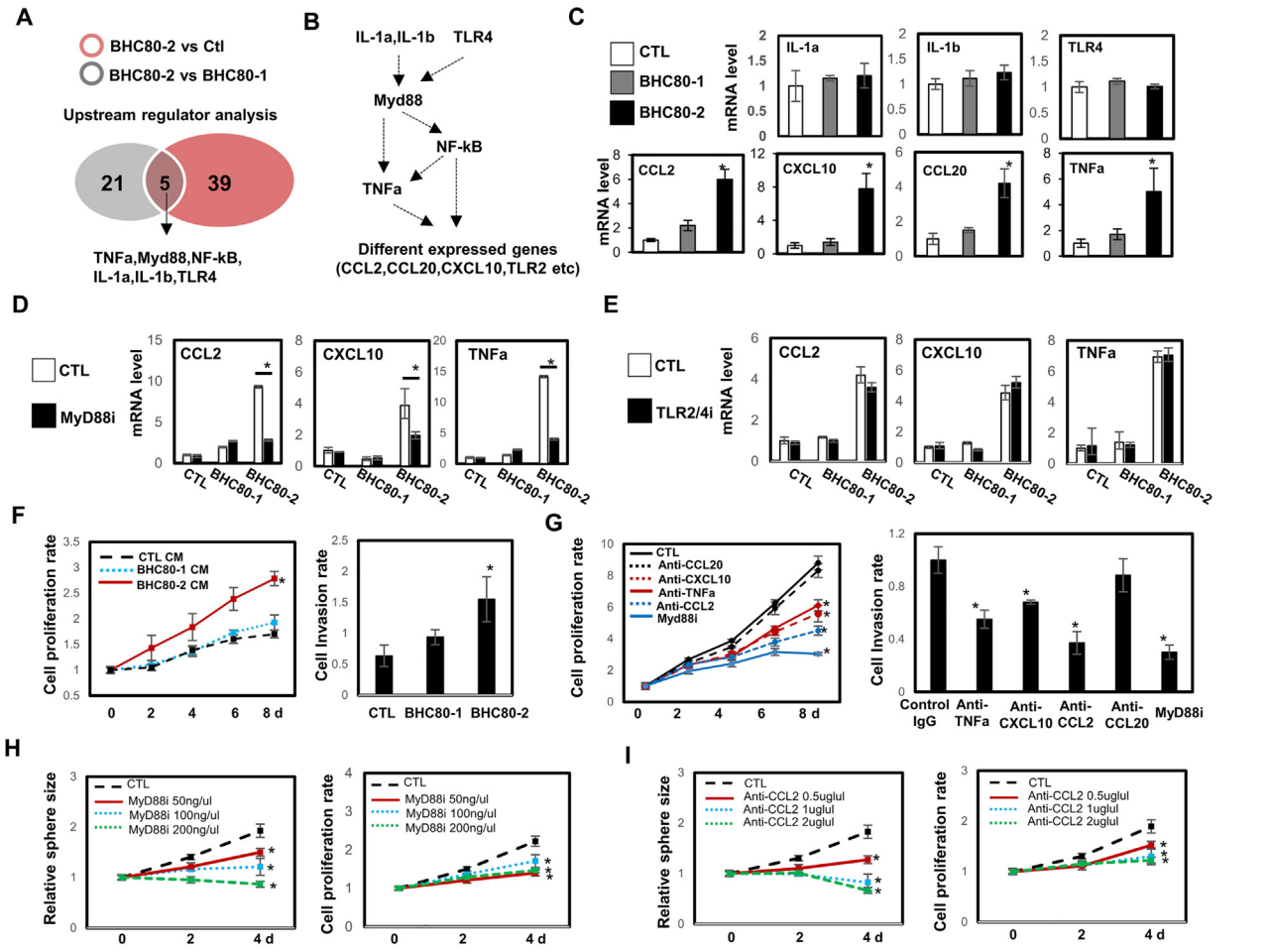

Fig. 4 – BHC80-2 targets the MyD88 signaling in PCa cells. (A) A Venn diagram shows the genes specifically regulated by BHC80-2 identified by gene microarray analyses. The IPA software predicted the common upstream regulators of BHC80-2 transcriptome (Z score > 2 and adjusted $p < 0.001$). (B) Interactions among five specific signals were predicted by IPA within the BHC80-2-specific transcriptome. (C) Genes specifically associated with BHC80-2 were validated by real-time qPCR. LNCaP(CTL), LNCaP(BHC80-1), and LNCaP(BHC80-2) cells were treated with (D) control or 100 ng/μl MyD88i inhibitory peptide (MyD88i) or (E) 30 μg/ml TLR2/4 inhibitor OxPAPC (TLR2/4i) for 24 h. CCL2, CXCL10, and TNFα mRNA levels were measured by real-time qPCR. (F) Conditioned media collected from LNCaP and PC3 cells overexpressing CTL; BHC80-1 and BHC80-2 were used to treat LNCaP or PC3 cells. LNCaP cell proliferation and PC3 invasion rates were measured. (G) LNCaP(BHC80-2) and PC3(BHC80-2) cells were treated with control, CCL2, CXCL10, TNFα, and CCL20 antibodies or the MyD88i. LNCaP(BHC80-2) cell proliferation and PC3(BHC80-2) cell invasion rates were measured. LNCaP(BHC80-2) spheroids were treated with (H) increasing doses of MyD88i or (I) CCL2 antibody for 0–4 d. Relative spheroids sizes and proliferation rates were measured during 0–4 d. All results were derived from three independent experiments that were performed in triplicate. Data are presented as the mean ± SD, with * delegating $p < 0.01$ when comparing with controls. IPA = Ingenuity Pathway Analysis; PCa = prostate cancer; qPCR = quantitative polymerase chain reaction; SD = standard deviation; TNFα = tumor necrosis factor alpha.

transcriptome was also analyzed by the Ingenuity Pathway Analysis (IPA) software. We identified tumor necrosis factor alpha (TNFα), MyD88, nuclear factor κ B (NFκB), interleukin (IL)-1a, IL-1b, and TLR4 (Z score > 2, $p < 0.001$) as the upstream regulators, and CCL2, CCL20, CXCL10, and TLR2 as downstream effectors (Fig. 4A and B). These bioinformatic predictions were validated by real-time polymerase chain reaction (PCR) in both LNCaP and PC3 cells, confirming that BHC80-2, but not BHC80-1, induced CCL20, CXCL10, CCL2, and TNFα expressions (Fig. 4C, and Supplementary Fig. 12F and G). In contrast, the expressions of IL-1a, IL-1b, and TLR4 were not changed. These results indicated that BHC80-2 may bypass IL-1a, IL-1b, and TLR4 to activate MyD88 and its downstream signaling. Further investigation showed that the MyD88 inhibitor (MyD88i), but not the TLR2/4 inhibitor, reduced BHC80-2 actions in upregulating CCL2, CXCL10, and TNFα (Fig. 4D and E). Conditioned media collected from LNCaP(BHC80-2) cells significantly enhanced LNCaP cell proliferation and PC3 invasion (Fig. 4F). Consistently, either CCL2, TNFα, and CXCL10 neutralizing antibodies or MyD88i treatment to LNCaP (BHC80-2) cells caused a reduction in cell proliferation (Fig. 4G). Furthermore, these treatments to PC3(BHC80-2) cells also suppressed cell invasion (Fig. 4G). LNCaP(BHC80-2) spheroid sizes and proliferation rates were suppressed by MyD88i and the CCL2 antibodies in a dose-dependent manner (Fig. 4H and I). Collectively, these results reveal a new function of BHC80-2 that can activate the MyD88 signaling to enhance CCL2, TNFα, and CXCL10 secretion, thereby stimulating PCa cell growth and invasion.

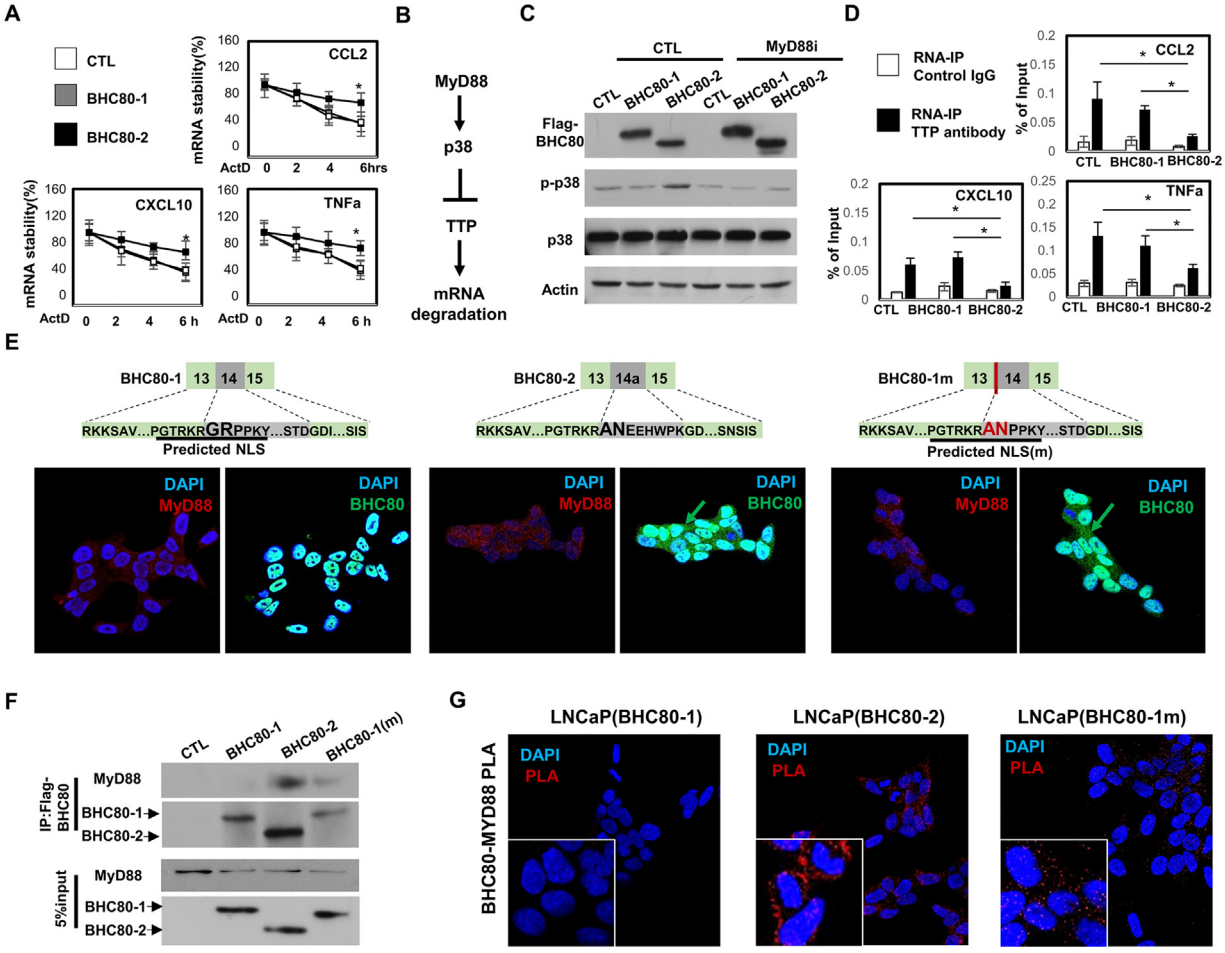

Fig. 5 – A novel nonepigenetic action of BHC80-2 triggers the MyD88-p38-TTP pathway. (A) LNCaP(CTL), LNCaP(BHC80-1), and LNCaP(BHC80-2) cells were treated with actinomycin D (ActD) for 0–6 h. CCL2, CXCL10, and TNFα mRNA levels were measured by real-time qPCR. (B) A schematic diagram shows MyD88 regulation of the stability of target RNAs by the MyD88-p38-TTP pathway. (C) LNCaP(CTL), LNCaP(BHC80-1), and LNCaP(BHC80-2) cells were incubated with control or Myd88i for 24 h. Phospho-p38 and total p38 protein levels were measured by immunoblotting. (D) In vivo RNA binding assays were performed using a TTP antibody. Eluted RNA fragments were used as templates for real-time qPCR. Signals were calculated as percentage of input. (E) Schematic diagrams of protein sequence differences among BHC80-1, BHC80-2, and BHC80-1m. LNCaP(BHC80-1), LNCaP(BHC80-2), and LNCaP(BHC80-1m) cells were used to perform immunofluorescence assays with BHC80 and MyD88 antibodies. (F) LNCaP(CTL), LNCaP(BHC80-1), LNCaP (BHC80-2), and LNCaP(BHC80-1m) cells were used to perform immunoprecipitation assays with the Flag tag antibody. The associated proteins were detected by MyD88 and Flag antibodies. (G) LNCaP(BHC80-1), LNCaP(BHC80-2), and LNCaP(BHC80-1m) cells were used to perform PLAs using BHC80 and MyD88 antibodies. All results were derived from three independent experiments that were performed in triplicate. Data are presented as the mean ± SD, with * delegating $p < 0.01$ when comparing with controls. One-way ANOVA followed by Tukey test was used in pairwise comparison among different groups. ANOVA = analysis of variance; NLS = nuclear localization signal; PLA = proximate ligation assay; qPCR = quantitative polymerase chain reaction; SD = standard deviation; TNFα = tumor necrosis factor alpha.

3.5. BHC80-2 activates MyD88-p38-TTP signaling through a novel nonepigenetic mechanism

We found that BHC80-2 regulated gene expression through two different mechanisms: (1) BHC80-2 enhanced the RNA stability of CXCL10, TNFα, and CCL2 (Fig. 5A and Supplementary Fig. 13A); and (2) BHC80-2 increased the transcription initiation rates of CCL20 and TLR2, demonstrated by nuclear run-on assays (Supplementary Fig. 13B). MyD88 was reported to stabilize CXCL10 and TNFα mRNAs in immune cells through the MyD88-p38-TTP pathway [27]. Specifically, MyD88 activates p38, which in turn reduces the affinity of TTP to its substrate RNAs and stabilizes cytokine mRNAs. We showed that BHC80-2 stimulated p38 phosphorylation; this effect was inhibited by MyD88i (Fig. 5B and C). The p38 inhibitor SB203580 (p38i) suppressed CXCL10, TNFα, and CCL2, but not CCL20 and TLR2 expressions induced by BHC80-2 (Supplementary Fig. 13C). In vivo RNA binding assays showed that BHC80-2 reduced TTP affinity to CXCL10, TNFα, and CCL2 mRNAs (Fig. 5D).

To determine whether the cytoplasmic actions of BHC80-2 were due to the disruption of the predicted NLS peptide by RNA splicing (Fig. 5E and Supplementary 14A), we applied immunofluorescence microscopy to show that BHC80-2 or BHC80-1 with mutations at the NLS (BHC80-1m, Gly429Asp, and Arg430Ala) was localized in both cytoplasm and nucleus, while BHC80-1 was expressed only in nucleus (Fig. 5E and Supplementary

Fig. 14A). These results were confirmed by immunoblotting assays using cytoplasm and nuclear fractions of LNCaP cells transfected with BHC80-1, BHC80-1m, and BHC80-2 (Supplementary Fig. 14B). Both coimmunoprecipitation and proximate ligation assays confirmed that BHC80-2 and BHC80-1m interacted with MyD88 in the cytoplasm (Fig. 5F and G, and Supplementary Fig. 14C). These results revealed a novel nonepigenetic action of BHC80-2. BHC80-2 is localized in cytoplasm to activate MyD88 and enhance the RNA stability of multiple tumor-promoting cytokines via the MyD88-p38-TTP axis.

3.6. Targeting of MyD88 signaling inhibits t-NEPC spheroid and tumor growth

To further confirm the key roles of BHC80-2-mediated MyD88 signaling during t-NEPC progression, we applied MyD88i and CCL2 neutralized antibodies to treat three NEPC spheroid models: DuNE, LnNE, and NCI-H660 spheroids. NEPC cells in vitro differ from AdPC cells in that they favor 3D growth condition in culture [12,13]. Both MyD88i and CCL2 antibodies suppressed spheroid growth according to spheroid size and proliferation rates (Fig. 6A).

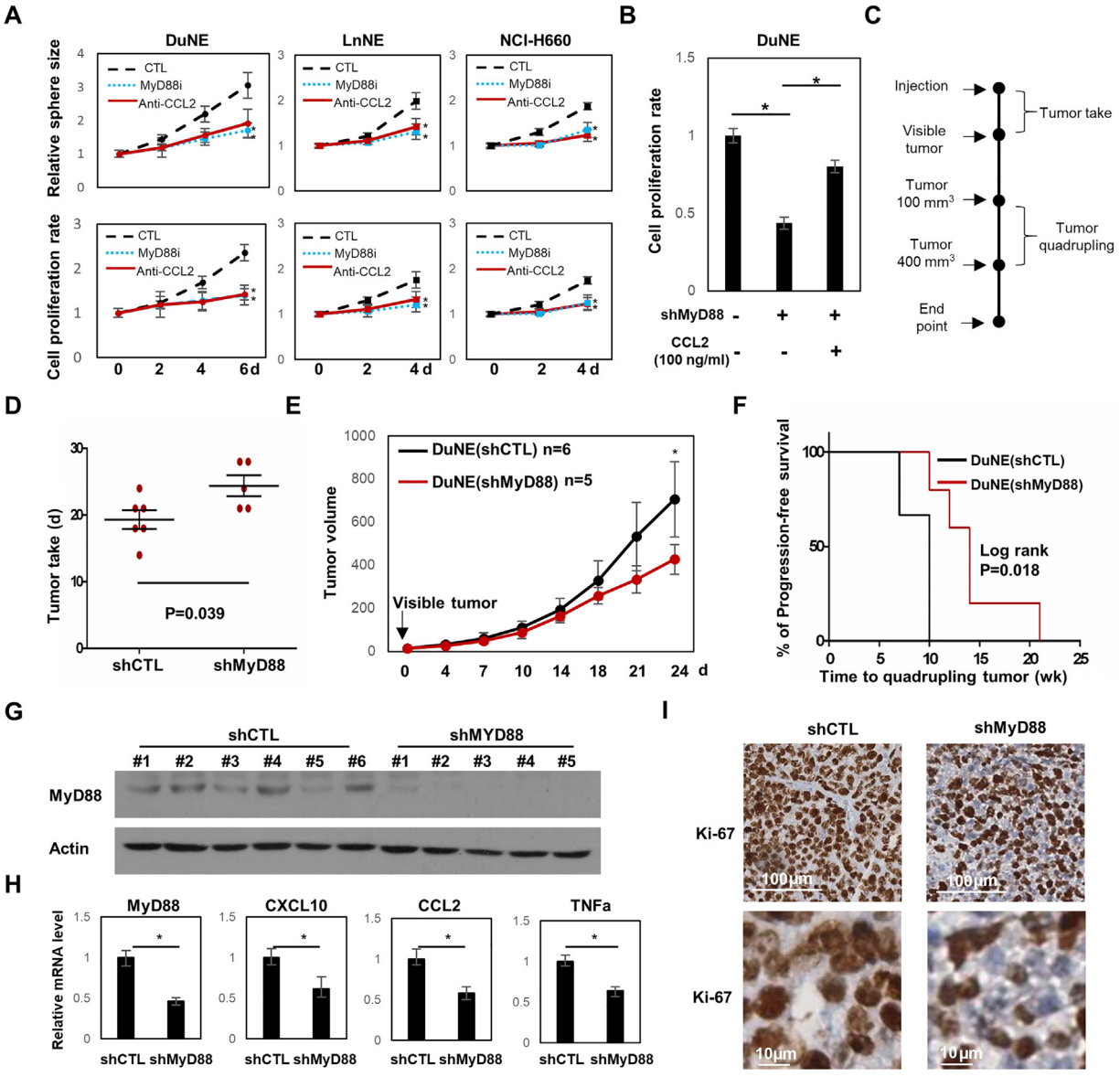

Fig. 6 – Blockade of BHC80-2 signaling inhibits NEPC cell spheroid and xenograft growth. (A) DuNE, LnNE, and NCI-H660 spheroids were treated with MyD88i or CCL2 antibody for 0–6 d. Relative spheroid sizes and proliferation rates were measured. (B) DuNE tumor cells were transduced with lentivirus encoding control or MyD88 shRNA. The transduced cells were used to measure proliferation rates under control or 100 ng/ml CCL2 protein treatment. (C) DuNE(shCTL) and DuNE(shMyD88) cells were used to generate DuNE xenografts in nude mice. A schematic diagram shows the experimental procedure of DuNE(shCTL) and DuNE(shMyD88) xenografts (Fig. 6B). (D) Tumor take, (E) tumor growth, and (F) tumor quadrupling time were measured. (G) Total protein lyses were collected from DuNE(shCTL) and DuNE(shMyD88) xenografts. MyD88 expression was confirmed by immunoblotting assays. (H) Total RNA from DuNE(shCTL) and DuNE(shMyD88) xenografts were extracted. The expression of MyD88, CCL2, CXCL10, and TNFα was measured by real-time qPCR. (I) Immunohistochemistry detected Ki-67 expression in DuNE(shCTL) and DuNE(shMyD88) xenografts. One-way ANOVA followed by Tukey test was used in pairwise comparison among different groups. Student *t* test was used to compare results between two groups, with * delegating $p < 0.01$ when comparing with controls. ANOVA = analysis of variance; qPCR = quantitative polymerase chain reaction; TNFα = tumor necrosis factor alpha.

MyD88 silencing to DuNE cells by shRNA inhibited cell proliferation; this effect can be rescued by CCL2 protein treatment (Fig. 6B). DuNE xenograft with MyD88 depletion showed delayed tumor take (Fig. 6C and D), inhibited tumor growth (Fig. 6E), and prolonged tumor quadrupling time (Fig. 6F). We confirmed that MyD88 depletion in xenografts was associated with reduced CCL2, CXCL10, and TNFα expressions, and a lower Ki67 index (Fig. 6G–I). These results support that blockade of BHC80-2-mediated MyD88 signaling inhibits NEPC cell spheroid and tumor growth.

4. Discussion

We report a novel nonepigenetic action of BHC80 that contributes to AdPC progression to t-NEPC. Functionally redirected by the neural splicing factor SRRM4, the splice variant of BHC80-2 is highly expressed in t-NEPC. BHC80-2 can be localized in the cytoplasm of cancer cells to trigger the MyD88-p38-TTP signaling, resulting in the stimulation of tumor-promoting cytokines, acceleration of cell proliferation, and androgen-independent tumor growth. These findings highlight key roles of RNA splicing mechanisms in regulating immune responses to counteract anticancer therapies and facilitate t-NEPC development.

The development of t-NEPC involves both differentiation and proliferation, two distinguishable and coordinated cellular processes controlled by multiple genes [28]. While NE differentiation is an initial step toward t-NEPC, proliferation is required for outgrowth of transdifferentiated cells and t-NEPC establishment. Detection of NE markers in AdPC cells is insufficient for a pathologist to diagnose NEPC and the Ki67 index, and morphological alterations are required to be confirmed. The significance of proliferation is even greater if proliferation driver genes specific to t-NEPC are identified and used to therapeutically target these progressive cell subpopulations. We showed that BHC80-2 splicing is t-NEPC specific and highly correlated with tumor cell morphology, NE marker status, and Ki67 index in patient tumors (Fig. 1). BHC80-2 stimulates androgen-independent cell proliferation and tumor progression (Fig. 3), highlighting that *BHC80*-2 is a proliferation driver gene for t-NEPC, and its mediated signaling may be potential therapeutic targets (Fig. 6).

BHC80 is a known component of histone demethylation complexes that regulate gene transcription [21]. However, no study has reported that BHC80-1 and BHC80-2 function differently. We define a novel nonepigenetic action unique to cytoplasmic BHC80-2 (Figs. 4 and 5). SRRM4-mediated RNA splicing of BHC80-2 destroys one of the NLSs, resulting in BHC80-2 cytoplasmic localization and activation of the MyD88-p38-TTP signaling (Figs. 2 and 5). While it cannot be excluded that the nuclear functions of BHC80-2 may contribute to t-NEPC development since BHC80-2 transcriptionally regulates CCL20 and TLR2, we demonstrated that the CCL20 neutralizing antibody did not antagonize BHC80-2-induced cell proliferation and invasion (Fig. 4G), and the TLR2/4 inhibitor did not alter CCL2, CXCL10, or TNFα expression (Fig. 4E), suggesting that the nuclear functions of BHC80-2 may not be essential for t-NEPC progression.

Our study established that BHC80-2-induced cytokines and inflammation contribute to t-NEPC progression. The adapter protein MyD88 is known to mediate various tumor-promoting signals triggered by microbial or endogenous ligands of cell surface receptors such as TLRs and IL-1Rs through downstream effectors such as NFκB, AKT, JNK, and p38 [27]. What we demonstrate here is that BHC80-2 bypasses cell surface receptors to activate MyD88 and stimulate cytokine expression. MyD88 induced its target gene expression by either enhancing the RNA stability or upregulating gene transcription initiation [29]. It is now clear that BHC80-2 enhances the RNA stability of CCL2, CXCL10, and TNFα through the MyD88-p38-TTP pathway (Figs. 4 and 5), and that these cytokines are key mediators for BHC80-2 to promote t-NEPC progression.

5. Conclusions

Alternative RNA splicing of BHC80-2 induces a novel nonepigenetic function that stimulates androgen-independent cell proliferation and tumor progression for t-NEPC development.

Author contributions: Xuesen Dong had full access to all the data in the study and takes responsibility for the integrity of the data and the accuracy of the data analysis.

Study concept and design: Dong.
Acquisition of data: Li, Xie, Lee, Lovnicki, Fazli.
Analysis and interpretation of data: Li, Zhang, Fazli, Huang.
Drafting of the manuscript: Dong, Chen, Huang.
Critical revision of the manuscript for important intellectual content: Dong, Huang, Gleave, Collins.
Statistical analysis: Li, Fazli.
Obtaining funding: Dong.
Administrative, technical, or material support: Xie, Lee, Lovnicki, Morrison, Musselman, Wang.
Supervision: Dong.
Other: None.

Financial disclosures: Xuesen Dong certifies that all conflicts of interest, including specific financial interests and relationships and affiliations relevant to the subject matter or materials discussed in the manuscript (eg, employment/affiliation, grants or funding, consultancies, honoraria, stock ownership or options, expert testimony, royalties, or patents filed, received, or pending), are the following: None.

***Funding/Support and role of the sponsor*:** This project is supported by a CIHR operating grant (MOP-137007 and PJT-156150) to Xuesen Dong, a China Scholar Council fellowship to Yinan Li, a CIHR graduate studentship to Ruiqi Chen, and TFRI New Frontiers Program Grant (#1062) for Martin Gleave, Colin Collins, and Xuesen Dong.

Acknowledgments: The authors would like to thank Estelle Li from the Pathology Core as well as Anne Haegert and Shawn Anderson from the Laboratory for Advanced Genome Analysis at the Vancouver Prostate Centre for their technical support-.

Appendix A. Supplementary data

Supplementary data associated with this article can be found, in the online version, at https://doi.org/10.1016/j.eururo.2019.03.011.

References

[1] Beltran H, Prandi D, Mosquera JM, et al. Divergent clonal evolution of castration-resistant neuroendocrine prostate cancer. Nat Med 2016;22:298–305.

[2] Palmgren JS, Karavadia SS, Wakefield MR. Unusual and underappreciated: small cell carcinoma of the prostate. Semin Oncol 2007;34:22–9.

[3] Mucci NR, Akdas G, Manely S, Rubin MA. Neuroendocrine expression in metastatic prostate cancer: evaluation of high throughput tissue microarrays to detect heterogeneous protein expression. Hum Pathol 2000;31:406–14.

[4] Aparicio A, Logothetis CJ, Maity SN. Understanding the lethal variant of prostate cancer: power of examining extremes. Cancer Discov 2011;1:466–8.

[5] Aparicio A, Tzelepi V, Araujo JC, et al. Neuroendocrine prostate cancer xenografts with large-cell and small-cell features derived from a single patient's tumor: morphological, immunohistochemical, and gene expression profiles. Prostate 2011;71:846–56.

[6] Lin D, Wyatt AW, Xue H, et al. High fidelity patient-derived xenografts for accelerating prostate cancer discovery and drug development. Cancer Res 2014;74:1272–83.

[7] Ku SY, Rosario S, Wang Y, et al. Rb1 and Trp53 cooperate to suppress prostate cancer lineage plasticity, metastasis, and antiandrogen resistance. Science 2017;355:78–83.

[8] Zou M, Toivanen R, Mitrofanova A, et al. Transdifferentiation as a mechanism of treatment resistance in a mouse model of castration-resistant prostate cancer. Cancer Discov 2017;7:736–49.

[9] Mu P, Zhang Z, Benelli M, et al. SOX2 promotes lineage plasticity and antiandrogen resistance in TP53- and RB1-deficient prostate cancer. Science 2017;355:84–8.

[10] Park JW, Lee JK, Sheu KM, et al. Reprogramming normal human epithelial tissues to a common, lethal neuroendocrine cancer lineage. Science 2018;362:91–5.

[11] Li Y, Donmez N, Sahinalp C, et al. SRRM4 drives neuroendocrine transdifferentiation of prostate adenocarcinoma under androgen receptor pathway inhibition. Eur Urol 2017;71:68–78.

[12] Lee AR, Gan Y, Tang Y, Dong X. A novel mechanism of SRRM4 in promoting neuroendocrine prostate cancer development via a pluripotency gene network. EBioMedicine 2018;35:167–77.

[13] Li Y, Chen R, Bowden M, et al. Establishment of a neuroendocrine prostate cancer model driven by the RNA splicing factor SRRM4. Oncotarget 2017;8:66878–88.

[14] Kim J, Jin H, Zhao JC, et al. FOXA1 inhibits prostate cancer neuroendocrine differentiation. Oncogene 2017;36:4072–80.

[15] Bang YJ, Pirnia F, Fang WG, et al. Terminal neuroendocrine differentiation of human prostate carcinoma cells in response to increased intracellular cyclic AMP. Proc Natl Acad Sci USA 1994;91:5330–4.

[16] Deeble PD, Murphy DJ, Parsons SJ, Cox ME. Interleukin-6- and cyclic AMP-mediated signaling potentiates neuroendocrine differentiation of LNCaP prostate tumor cells. Mol Cell Biol 2001;21:8471–82.

[17] Qi J, Nakayama K, Cardiff RD, et al. Siah2-dependent concerted activity of HIF and FoxA2 regulates formation of neuroendocrine phenotype and neuroendocrine prostate tumors. Cancer Cell 2010;18:23–38.

[18] Mosquera JM, Beltran H, Park K, , et al. Concurrent AURKA. and *MYCN* gene amplifications are harbingers of lethal treatment-related neuroendocrine prostate cancer. Neoplasia 2013;15:1–10.

[19] Tsai H, Morais CL, Alshalalfa M, et al. Cyclin D1 loss distinguishes prostatic small-cell carcinoma from most prostatic adenocarcinomas. Clin Cancer Res 2015;21:5619–29.

[20] Beltran H, Rickman DS, Park K, et al. Molecular characterization of neuroendocrine prostate cancer and identification of new drug targets. Cancer Discov 2011;1:487–95.

[21] Lan F, Collins RE, De Cegli R, et al. Recognition of unmethylated histone H3 lysine 4 links BHC80 to LSD1-mediated gene repression. Nature 2007;448:718–22.

[22] Iwase S, Januma A, Miyamoto K, et al. Characterization of BHC80 in BRAF-HDAC complex, involved in neuron-specific gene repression. Biochem Biophys Res Commun 2004;322:601–8.

[23] Li Y, Zhang Q, Lovnicki J, et al. *SRRM4* gene expression correlates with neuroendocrine prostate cancer. Prostate 2019;79:96–104.

[24] Raj B, Irimia M, Braunschweig U, et al. A global regulatory mechanism for activating an exon network required for neurogenesis. Mol Cell 2014;56:90–103.

[25] Calarco JA, Superina S, O'Hanlon D, et al. Regulation of vertebrate nervous system alternative splicing and development by an SR-related protein. Cell 2009;138:898–910.

[26] Kaplan-Lefko PJ, Chen TM, Ittmann MM, et al. Pathobiology of autochthonous prostate cancer in a pre-clinical transgenic mouse model. Prostate 2003;55:219–37.

[27] Sun D, Ding A. MyD88-mediated stabilization of interferon-gamma-induced cytokine and chemokine mRNA. Nat Immunol 2006;7:375–81.

[28] Chen R, Dong X, Gleave M. Molecular model for neuroendocrine prostate cancer progression. BJU Int 2018;122:560–70.

[29] Narayanan KB, Park HH. Toll/interleukin-1 receptor (TIR) domain-mediated cellular signaling pathways. Apoptosis 2015;20:196–209.